Hermann-Föttinger-Institut für Strömungsmechanik
Technische Universität Berlin

Institutsbericht Nr. 05/98

A Fundamental Study of Duct Acoustics via Computational Aeroacoustics Approach

X.D. Li[1] , L.P., Xue, J.P., Yan, F. Thiele

[1]Department of Jet Propulsion, Beijing University of Aeronautics and Astronautics

Contents

List of Figures

1 ABSTRACT

Based on solving the two-dimensional linearized Euler equations in terms of acoustic disturbances in generalized curvelinear coordinates, a parallelized multi-domain two-dimensional computational aeroacoustic code is developed. The dispersion-relation-preserving (DRP) scheme has been used for spatial discretization while the low dispersion and low dissipation Runge-Kutta (LDDRK) scheme has been used for time integration. The radiation and outflow boundaries based on asymptotic solutions have been used in the far-field boundaries. This code has been validated by several benchmark problems from the second CAA workshop including the cylinder scattering, the sound radiation from a point source at the center of the duct and the sound radiation from a duct inlet. It is intended to use the code developed to investigate the geometrical effects of a duct inlet.

2 Introduction

Duct acoustics has gained great interests for its various applications in industry such as aircraft engines. During the past few decades various theoretical and numerical methods have been developed to study duct acoustics. These traditional methods can be categorized into four groups: (i)analytical method, e.g., Mani[13]; (ii) finite element method using the wave envelope technique, e.g., Everman *et al* [4] [16]; (iii) boundary element method, e.g. [14]; (iv) finite difference method, e.g. [7].

With consideration of the features of the duct inlet geometry and physics in and around it associated with the background flow and sound waves, the analysis of their propagation and radiation by analytical tools and simplified numerical approaches can not be used to more accurate and insightful predictions. Numerical solutions from higher-levels equations are needed to properly model most of the physics mentioned above. The emergence of powerful parallel computers has recently let to include more physical phenomena in the numerical simulations of aeroacoustic problems by solving the full Euler or Navier-Stokes equations. This newly emerging and fast growing field is known as computational aeroacoustics (CAA).

Recently, researchers at Pennsylvania State university computed the sound radiation from a realistic engine inlet by a hybrid CAA code with prescribed sources from the fan[15]. The code solves the three-dimensional full Euler equations to determine the near-field acoustics and uses a moving surface Kirchhoff formula to predict the far-field noise. In general the unsteady flow field (ρ, u, v, w, p) is described by a steady state mean flow $(\bar{\rho}, \bar{u}, \bar{v}, \bar{w}, \bar{p})$ and an unsteady disturbance (ρ', u', v', w', p') which are connected through $u = \bar{u} + u'$, etc. The flow solver uses an explicit, spatially and temporally fourth-order accurate, finite difference, Runge-Kutta (R-K) time-integration scheme. Once the steady-state solution for the mean flow variables is obtained, the time-accurate inlet fan-face conditions (acoustic sources) are turned on which allows to advance the solutions in a time-accurate manner for ρ, u, v, w, p. This procedure inherently requires that the same scheme has to be used to evaluate the residuals of the governing equations in both the steady and unsteady calculations. Starting from the steady solution the time integration is smooth and no spurious waves are generated. However, there are several difficulties associated with using a high-order explicit scheme for steady-state calculations. The fourth-order scheme is really designed for time-accurate problems with low dissipation and dispersion. In other words, low-frequency modes are not damped out. Moreover, typical turbofan inlet radiation problems involve high blade-passing frequencies (BPF). Hence, very fine meshes are usually needed which result in very small time steps and consequently slow convergence. Also, turbofan noise predictions are often made at low freestream Mach numbers associated with landing or takeoff conditions, which are considered more citical in terms of community noise regulations. The disparity of the eigen-values in these cases is a degrading factor in achieving sufficiently rapid steady-state solutions. Although the multigrid technique has been used to accelerate the solution to steady-state some more efficient techniques are still desirable.

A more direct CAA approach[3] was developed by NASA Lewis Research Center. The axisymmetric Euler equations in generalized curvilinear coordinates were solved by the Dispersion-Relation-Preserving (DRP) finite difference scheme whereas the far-field was computed by the Kirchhoff formula. From the view point of real applications, this approach is still too time consuming. Nevertheless, these advances have shed lights on further understanding of duct acoustics by using CAA methods.

Very recently, some European countries have also started some research work on CAA, such as in Germany[12], France[5]. However, more extensive investigations with respect to the real applications of CAA are greatly required in Eurropean countries.

The long term goal of this research is to develop a three-dimensional CAA code for simulating the sound radiation and propagation process around the real aero-engine inlet. The investigation presented here are restricted to two-dimensional cases in order to study at the very beginning some fundamental CAA problems for duct acoustics. The most concerned technical issue were concentrated on various boundary conditions (BC) including the curved solid wall BC, the far-field BC and the radiation BC inside a duct. Other technical issues concerned were multi-block grid generations with non-uniform grid distribution in each block and parallel computations. The CAA code developted has been validated by several benchmark problems from the second CAA workshop[17].

3 Numerical Algorithm

3.1 Governing Equations

The solution of the unsteady 3D NS equations would lead to complete discrption of the whole flow field including the acoustics. However this requires a time and space accurate integration of the governing equation by DNS which is only possible for very simple flow configurations even with the use of super computers presently avalable. considering aeroacoustic problems of engineering importance the DNS is not visible even in the near future the perturbation technique is applied here, e.g. specify $u = \bar{u} + u'$.

Perturbation technique consists

- solve full NS/Euler for mean flow $\bar{\rho}, \bar{u}, \bar{v}, \bar{w}, \bar{p}$.
- solve disturbance equations (linear or nonlinear) for perturbation variables ρ', u', v', w', p'.

Here restriction to the linear disturbance approach.

The linearized, two-dimensional, compressible, Euler equtions are used as the governing equations. With an option for Cartesian or cylindrical coordinates, the equations (with source term $\mathbf{H}$) sets are written as

$$\frac{\partial \mathbf{U}}{\partial t} + \frac{\partial \mathbf{E}}{\partial x_1} + \frac{\partial \mathbf{F}}{\partial x_2} + \frac{m\mathbf{G}}{r^m} = \mathbf{H} \tag{1}$$

where $m = 0$ for the Cartesian coordinate system, $(x_1, x_2) = (x, y)$, and $m = 1$ for the cylindrical coordinate system, $(x_1, x_2) = (x, r)$, and

$$\mathbf{U} = \begin{bmatrix} \rho' \\ u' \\ v' \\ p' \end{bmatrix}, \quad \mathbf{E} = \begin{bmatrix} M_{x_1}\rho' + u' \\ M_{x_1}u' + p' \\ M_{x_1}v' \\ M_{x_1}p' + u' \end{bmatrix}, \quad \mathbf{F} = \begin{bmatrix} M_{x_2}\rho' + v' \\ M_{x_2}u' \\ M_{x_2}v' + p' \\ M_{x_2}p' + v' \end{bmatrix}, \quad \mathbf{G} = \begin{bmatrix} v' \\ 0 \\ 0 \\ v' \end{bmatrix}$$

in which, M_{x_1} and M_{x_2} are constant mean flow Mach number in the x_1 and x_2 direction, respectively.

In order to use the body fitted computational meshes the governing equations are transformed to the generalized curvilinear coordinates as

$$\frac{\partial \hat{\mathbf{U}}}{\partial t} + \frac{\partial \hat{\mathbf{E}}}{\partial \xi} + \frac{\partial \hat{\mathbf{F}}}{\partial \eta} + \frac{m\hat{\mathbf{G}}}{r^m} = \hat{\mathbf{H}} \tag{2}$$

where

$$\hat{\mathbf{U}} = J[\rho', u', v', p']^T \quad , \quad \hat{\mathbf{E}} = J[\xi_{x_1}\mathbf{E} + \xi_{x_2}\mathbf{F}] \quad , \quad \hat{\mathbf{F}} = J[\eta_{x_1}\mathbf{E} + \eta_{x_2}\mathbf{F}]$$

$$\hat{\mathbf{G}} = J\mathbf{G} \quad , \quad \hat{\mathbf{H}} = J\mathbf{H}$$

The metric Jacobian J is defined by $J = \partial(x_1, x_2)/\partial(\xi, \eta)$.

3.2 Discretization Schemes

Recent work has shown that the numerical discretization schemes in both space and time should be optimized for a wider range of effective wave number but do not deviate from the physics. Here, the 7-point dispersion-relation-preserving (DRP) scheme proposed by Tam and Webb[19] has been used for spatial discretization whereas a 4-6 optimized low-dissipation and low-dispersion Runge-Kutta (LDDRK) scheme [9] has been applied for time integration.

3.3 Boundary Conditions

3.3.1 Radiation Boundary Conditions

At the outer boundary where there are only outgoing acoustic waves the radiation boundary conditions should be applied. Under the assumption of steady state mean flow, the asymptotic radiation boundary conditions due to Bayliss & Turkel[1] and Tam & Webb[19] can be described as

$$\left(\frac{1}{V(\theta)}\frac{\partial}{\partial t}+\frac{\partial}{\partial r}+\frac{1}{2^{(1-m)}r}\right)\begin{bmatrix}\rho'\\ u'\\ v'\\ p'\end{bmatrix}=0 \tag{3}$$

where $m=0$ and $m=1$ are for two and three dimensional cases, respectively. Here $V(\theta)=a_\infty[M\cos\theta+(1-M^2\sin^2\theta)^{1/2}]$, $M=\sqrt{M_{x_1}^2+M_{x_2}^2}$, r is measured from the center of acoustic sources and θ is the angular coordinate of boundary points.

3.3.2 Outflow Boundary Conditions

At the outflow region the outgoing disturbances consist of a combination of acoustic, entropy and vorticity waves. Assuming the uniform mean flow $\bar{u}$, the asympotic outflow boundary conditions [19] are

$$\begin{aligned}
&\frac{\partial\rho'}{\partial t}+\bar{u}\frac{\partial\rho'}{\partial x_1}=\frac{1}{a_\infty^2}\left(\frac{\partial p'}{\partial t}+\bar{u}\frac{\partial p'}{\partial x_1}\right)\\
&\frac{\partial u'}{\partial t}+\bar{u}\frac{\partial u'}{\partial x_1}=-\frac{1}{\bar{\rho}}\frac{\partial p'}{\partial x_1}\\
&\frac{\partial v'}{\partial t}+\bar{u}\frac{\partial v'}{\partial x_1}=-\frac{1}{\bar{\rho}}\frac{\partial p'}{\partial x_2}\\
&\frac{1}{V(\theta)}\frac{\partial p'}{\partial t}+\frac{\partial p'}{\partial r}+\frac{p'}{2^{(1-m)}r}=0
\end{aligned} \tag{4}$$

where $m=0$ and $m=1$ are for two and three dimensional cases, respectively.

3.3.3 Solid Wall Boundary Conditions

For the curved solid wall, the slip boundary condition is imposed which requires that the normal contravariant velocty is to be set to zero:

$$\vec{V} \cdot n_{wall} = \eta_x u + \eta_y v = 0 \tag{5}$$

The numerical approach based on the ghost value by Tam and Dong[21] is applied to the above equation (5). For each ξ on the wall, a ghost value of p is chosen such that this equation is satisfied.

3.3.4 Duct Inlet Inner Face Boundary Condition

The radiation boundary condition imposed at the inlet inner face of a duct must have two functions. First, it simulates a noise source to generate the incoming duct acoustic wave modes propagating towards the open end. Second, it allows the acoustic waves reflected from the open end to leave the computational domain smoothly. Several different methods have been proposed to serve this purpose [18] [10] [2] [3]. Here, we use the same procedure as Dong *et al* [2] [3] to construct the duct inlet inner face boundary condition. In the region of the duct away from the open end, the acoustic solution consists of the incident and reflected waves, that is

$$p' = p'_{in} + p'_{re} \tag{6}$$

Assuming a single angular frequency ω, the reflected wave modes must be of the form

$$p'_{re} = \sum_{m,n} p'_{mn} J_m(\mu_{mn} r) e^{(ik_{mn}x + m\theta - \omega t)} \tag{7}$$

where m is the circumferential mode number and μ_{mn} is the radial mode eigenvalue.

The axial wave number k_{mn} can be computed from the dispersion relation

$$\frac{k^{\pm}_{mn}}{\omega} = \frac{1}{1 - M_x^2}\left[-M_x \pm \sqrt{1 - (1 - M_x^2)\left(\frac{\mu_{mn}}{\omega}\right)^2}\right] \tag{8}$$

where k^{+}_{mn} and k^{-}_{mn} represents waves propagating downstream and upstream, respectively. For $\mu_{mn}\sqrt{1 - M_x^2}/\omega \leq 1$, $k^{\pm}_{mn}$ are real. Waves propagate both upstream and downstream without attenuation (cut-on). For $\mu_{mn}\sqrt{1 - M_x^2}\omega > 1$, $k^{\pm}_{mn}$ are a pair of conjugate complex numbers. Waves in both directions are attenuated exponetially with distance (cut-off).

Differentiating equation (6) (7) with respect to x and t yields

$$\frac{\partial p'}{\partial x} = \frac{\partial p'_{in}}{\partial x} + i \sum_{m,n} k_{mn} p'_{mn} J_m(\mu_{mn} r) e^{(ik_{mn}x + m\theta - \omega t)} \tag{9}$$

and

$$\frac{\partial p'}{\partial t} = \frac{\partial p'_{in}}{\partial t} - i\omega p'_{re} \tag{10}$$

At the duct inner face boundary region, only the cut-on modes of the reflected waves are considered. By using a Taylor series approximation, the reflected axial wave number can be expressed as

$$k_{mn} = \frac{\omega}{1 - M_x^2}\left[-M_x - 1 - O\left((1 - M_x^2)\left(\frac{\mu_{mn}}{\omega}\right)^2\right)\right] = \frac{\omega}{M_x - 1} \tag{11}$$

By combining equation (9)–(11), the duct inner face boundary condition for p' can be written as

$$\frac{\partial p'}{\partial t} + (M_x - 1)\frac{\partial p'}{\partial x} = \frac{\partial p'_{in}}{\partial t} + (M_x - 1)\frac{\partial p'_{in}}{\partial x} \tag{12}$$

Using a similar procedure, the boundary conditions for ρ', u', v' can also be obtained. Here it should be mentioned that there are some typing errors in the corresponding equation (12) of ref. [2] [3].

3.4 Artificial Damping

It is well known that the DRP scheme and all the other high-order finite difference schemes support short wavelength spurious numerical waves. These spurious waves are often generated at various computational boundaries (solid wall, far-field, duct inner face) and by nonlinearities. In order to obtain a high quality numerical solution, the short wavelength spurious waves should be eliminated. Here, the method of Tam *et al* [20] has been adopted for artificial damping. The basic idea can be introduced by considering the linearized u-momentum equation. Add a linear damping term to the right side of this equation and use the 7-point stencil for discretization. Then the discretized equation at the mesh point l can be written as

$$\frac{du_l}{dt} + \cdots = -\frac{\nu_a}{(\Delta x)^2}\sum_{j=-3}^{3} d_j u_{l+j} \tag{13}$$

where $[\nu_a/(\Delta x)^2]$ is the damping coefficient.

The magnitude of the added artificial damping term is evaluated by the artificial mesh Reynolds number which is defined as $Re_{\Delta x} = a_\infty \Delta x/\nu_a$.

3.5 Parallization

With respect to CPU time and memory requirement, parallization techniques are almost mandatory for real aeroacoustics problems. The available CAA code has been parallelized using a domain decomposition technique. The computational domain is divided into several blocks of regular structure. For each block the solution is performed on a single processor of either a distributed memory workstation cluster or an MPP, like the CRAY T3E. A flexible interprocessor communication, depending on the considered platform, is implemented by applying the standard PVM message passing system or highly efficient platform-related routines (like $shmem\_put/get$ on the CRAY T3E). Efficiency measurements show an almost linear increase in speed.

3.6 Grid Generation

It is very important to generate suitable grids for CAA and CFD computations. In general the requirements for the generation of suitable grids with respect to CFD and CAA are quite different. Hence CFD and CAA should not use the same grid system e.g. as highly accurae integration schemes are required for the solution of the disturbance equation. For CFD calculation the grid generation has to account for the flow geometry considered as well as the flow physics e.g. turbulence. Very advanced solution procudures on available to calculate the mean flow, for example finite volume based ELAN. Generally, uniformly distributed cartesian grids are most suitable for large distance wave propagation in CAA. However, they are rather difficult to handle in complex applications because it is rather difficult to implement the solid wall boundary conditions for complex geometries[11]. For this reason, body-fitted grids are chosen for the CAA computations. This approach offers high flexibility for the formulation of the solid wall boundary conditions and the description of complex geometries. In addition, it is relatively easier to be coupled with most of the available CFD codes which are based on the body-fitted grids.

Besides, an overlapping grid generation technique due to high accuracy and the coding on parallel computers has been used to generate block-structured grids in order to be suitable for parallel computations. The overlapping zones are used for data exchange between different processors depends on the discretization scheme in space . As mentioned above the CAA grids should be as uniformly distributed as possible, particularly near the boundary regions, such as the solid wall, or in the far-field.

4 Numerical Examples

In order to test the CAA code, three benchmark problems from the second CAA workshop[17] have been chosen for validation. The main purpose is to test various numerical boundary conditions. Particular attention has been paid to the curved solid wall boundary conditions, duct inlet inner boundary conditions and far-field boundary conditions.

4.1 Acoustic Scattering by a Circular Cylinder

The benchmark problem of category 1 (probelm 2) from the second CAA workshop[17] has been chosen for testing curved wall boundary conditions. The physical problem is to simulate the sound field generated by a propeller scattered off by the fuselage of an aircraft. The fulelage and the noise source (propeller) have been idealized as a cirlular cylinder and a line source, respectively. The computational domain is shown in Fig.1. An initial value problem with no mean flow is considered to be solved with initial conditions $t = 0, u = v = 0$, and

$$p' = \exp\left[-\ln 2\left(\frac{(x-4)^2 + y^2}{0.2^2}\right)\right]$$

The asymptotic radiation boundary conditions are applied on the outer boundary of the computational domain. The solid wall boundary conditions are used on the curved solid wall of the cylinder.

As the problem is symmetric about the x-axis, only the upper half $x - y$-plane will be considered for the numerical solution. And a symmetric boundary condition is imposed at $y = 0$. For the results presented below, $\Delta r == 0.03$ and $\Delta\theta = 1^0$. Time step is $\Delta t \approx 0.00658$.

Fig.2 shows the instantaneous pressure contours at time $t = 4$. There are two main wave fronts. One is created by the initial pulse. Another one is reflected off the right surface of the cylinder facing to the initial pulse. Fig.3 gives the results at time $t = 7$ which shows that a relatively weak third wave front is generated by the collision and merging of the splitted two initial wave fronts due to the cylinder. Fig.4 shows the time history of pressure fluctuation at three chosen points A ($r = 5, \theta = 90°$), B ($r = 5, \theta = 135°$), C ($r = 5, \theta = 180°$). The numerical results agrees rather well with exact time histories.

4.2 Radiation of Sound from a Point Source in a Duct

The benchmark problem of category 2 (probelm 1) from the second CAA workshop [17] has been chosen for calculating sound radiation for a both-end-open cylindrical duct. The computational domain is shown in Fig.5. In this problem, the mean Mach number is 0.5 parallel to the duct axis. A harmonic source with a narrow Gaussian spatial distribution is located at the center of the duct and given by

$$H = 0.1\exp\left[-48(ln2)\left(\frac{kD}{2\pi}\right)^2(x^2 + r^2)\right]\cos(kDt)$$

For the numerical results presented, the angular frequency $\omega = 2\pi f = 4.409507\pi$ is used. Since it is a axisymmetric probelm, only the upper half domain has to be considered for computation. Symmtric boundary conditions are imposed along the duct axis. Four blocks have been used for computation with the mesh size as $\Delta x = D/51$ and $\Delta r = D/50.5$. The grid points nearest to duct axis have used half grid size along radial direction in order to avoid singularities. The time step size $\Delta t = 0.005$. A instantaneous pressure contours at time $t = 80$ is shown in Fig.6. It can be clearly seen that the radiation patterns between the upstream and downstream of the duct are unsymmetric with the mean flow convection effects. After long time integration, the computation become periodic. Fig.7 shows the far-field radiation directivity which is represented by the RMS pressure $\bar{p}^2$. These results agrees rather well the results presented by other groups[17].

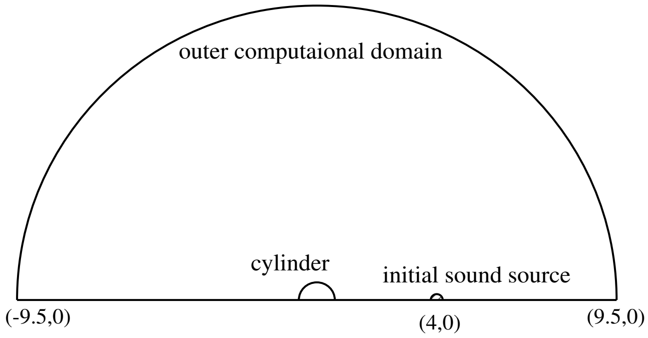

Figure 1: Computational domain for acoustic scattering by a cylinder.

4.3 Radiation of Sound from a Duct Inlet

The benchmark problem of category 2 (probelm 2) from the second CAA workshop [17] has been chosen for calculating sound propagation through a semi-infinite circular duct and its radiation to an unbounded space. The computational domain is shown in Fig.8. The incoming acoustic waves are specified at the inner face of the duct as

$$\begin{bmatrix} \rho' \\ u' \\ v' \\ p' \end{bmatrix}_{in} = \Re \left\{ \begin{bmatrix} J_m(\mu_{mn} r) \\ \frac{(\omega^2-\mu_{mn}^2)^{1/2}}{\omega} J_m(\mu_{mn} r) \\ \frac{-i\mu_{mn}^2}{\omega} J_m'(\mu_{mn} r) \\ J_m(\mu_{mn} r) \end{bmatrix} \times e^{i[(\omega^2-\mu_{mn}^2)^{1/2}x+m\theta-\omega t]} \right\} \tag{14}$$

where m is the circumferential and n is the radial mode numbers. $m = 0$ and $n = 2$ are specified in the computations. Two cases for $\omega = 10.3, 7.2$ are computed. Three blocks have been used for parallel computations. The uniformly distributed grid size are chosen with $\Delta x = 1/16$ and $\Delta r = 1/15.5$. In order to avoid singularitis, half grid size along r direction has been for the grid line nearest to duct axis. The time step size $\Delta t = 0.0303$. Fig.9 gives the instantaneous pressure contours for $\omega = 10.3$ at time $t = 140$. The far-field directivity $D(\theta) = \lim_{R\to\infty} \overline{R^2 p^2(R, \theta, \phi, t)}$ is given in Fig.10. The pressure envelop $P'(x) = \max_{overtime} p'(r, \phi, x, t)$ inside the duct along the four radial lines $r = 0, 0.34, 0.55, 0.79$ is shown in Fig.11. The corresponding numerical results for $\omega = 7.2$ case are shown in Fig.12 to Fig.14. Comparing with results by other groups, the presented solutions agrees well in general.

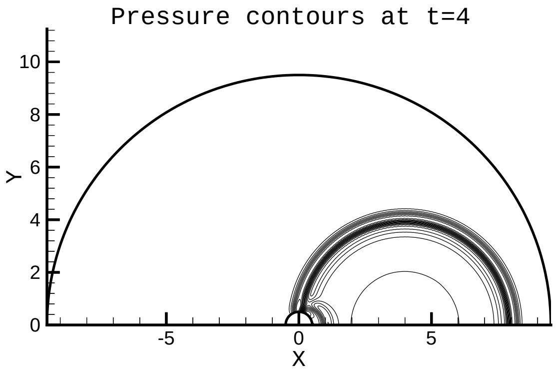

Figure 2: Instantaneous pressure contours of acoustic scattering off a cylinder at $t = 4$.

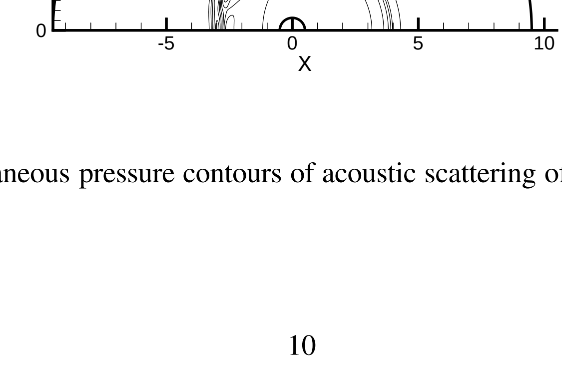

Figure 3: Instantaneous pressure contours of acoustic scattering off a cylinder at $t = 7$.

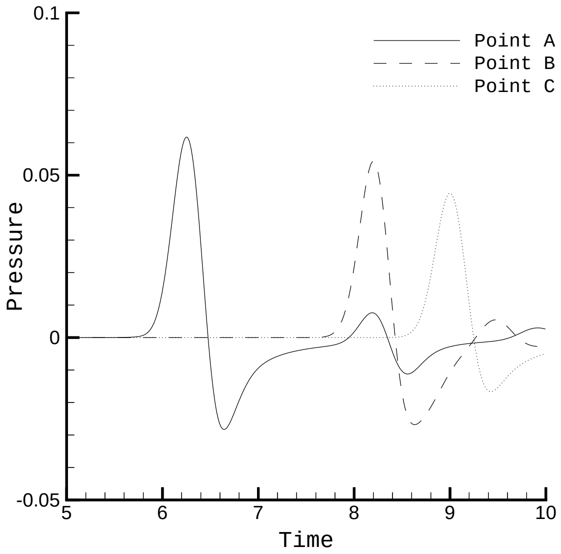

Figure 4: Time history of pressure fluctuation. (a)A ($r = 5, \theta = 90°$), (b)B ($r = 5, \theta = 135°$), (c)C ($r = 5, \theta = 180°$).

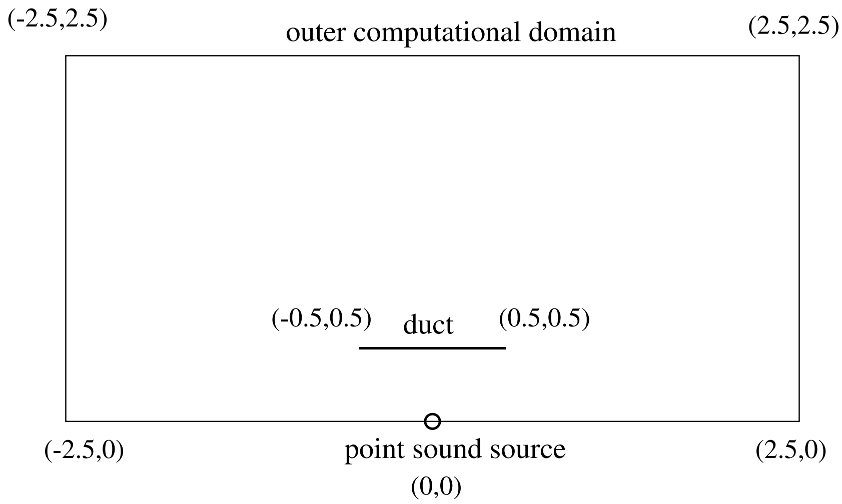

Figure 5: Computaional domain for sound scattering from a point sound source at the center of a duct.

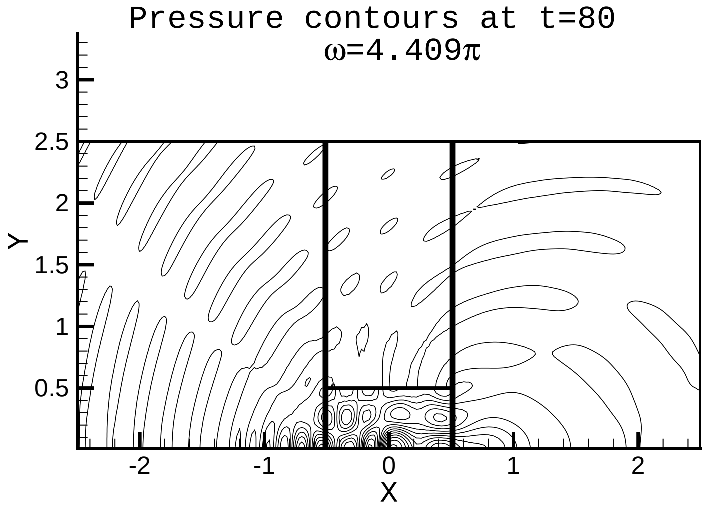

Figure 6: Instantaneous pressure contours for $kD = 4.409\pi$ at $t = 80$.

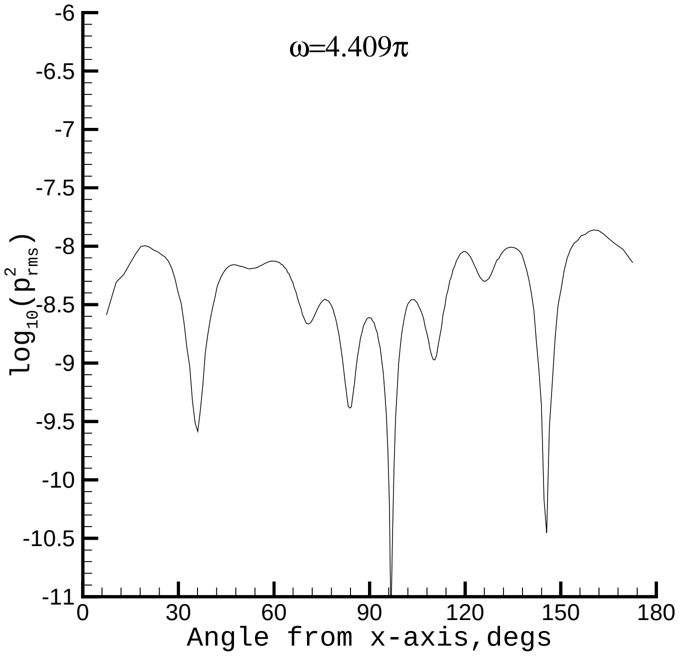

Figure 7: RMS pressure along $r = 2.5$ for $kD = 4.409\pi$.

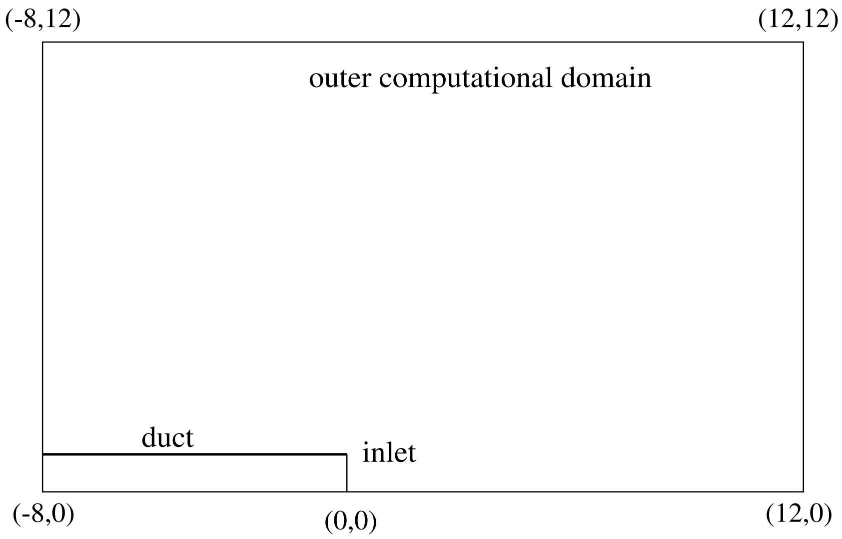

Figure 8: Computaional domain for sound radiation from a duct inlet.

5 Conclusion

Some fundamental studies have been conducted on the application of computational aeroacoustics approach to duct acoustics. The numerical boundary conditions for curved solid wall, far-field, and duct inlet inner face have been tested. Since the governing equations are solved in generalized curvilinear coordinates system. The available CAA code is expected to solve aeroacoustic problems with complex geometries which is now in progressing.

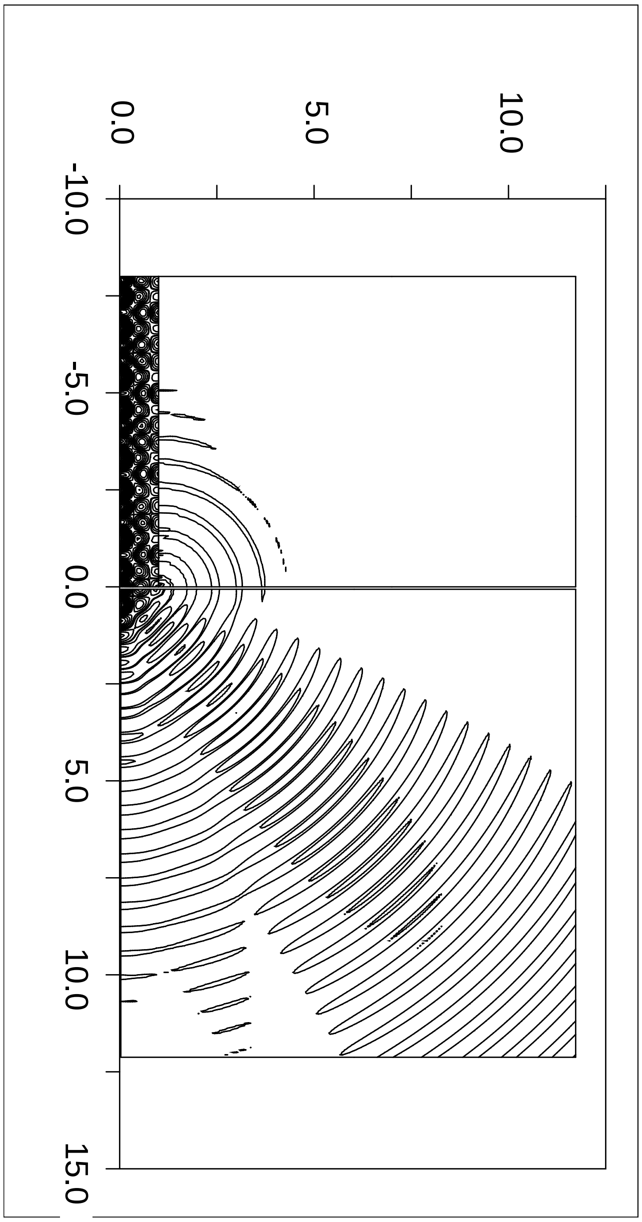

Figure 9: Instantaneous pressure contours for $\omega = 10.3$ at $t = 140$.

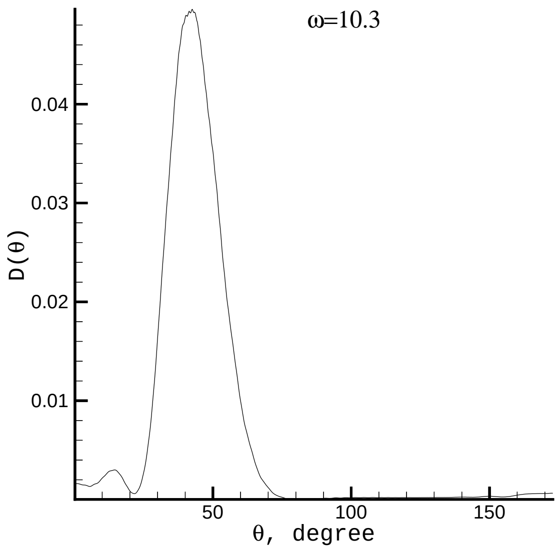

Figure 10: Far field directivity for $\omega = 10.3$.

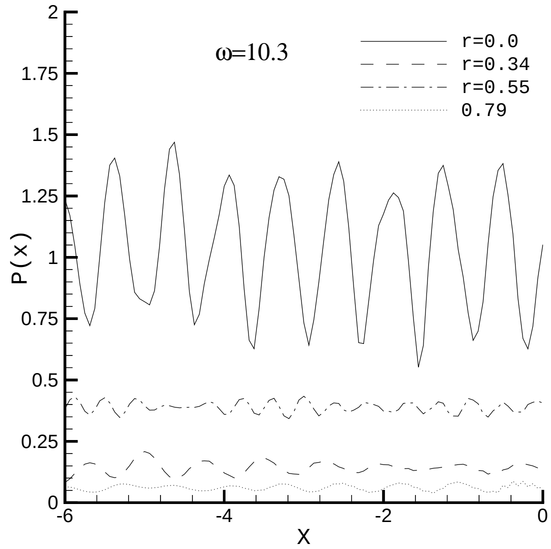

Figure 11: Wave envelope inside a duct for $\omega = 10.3$.

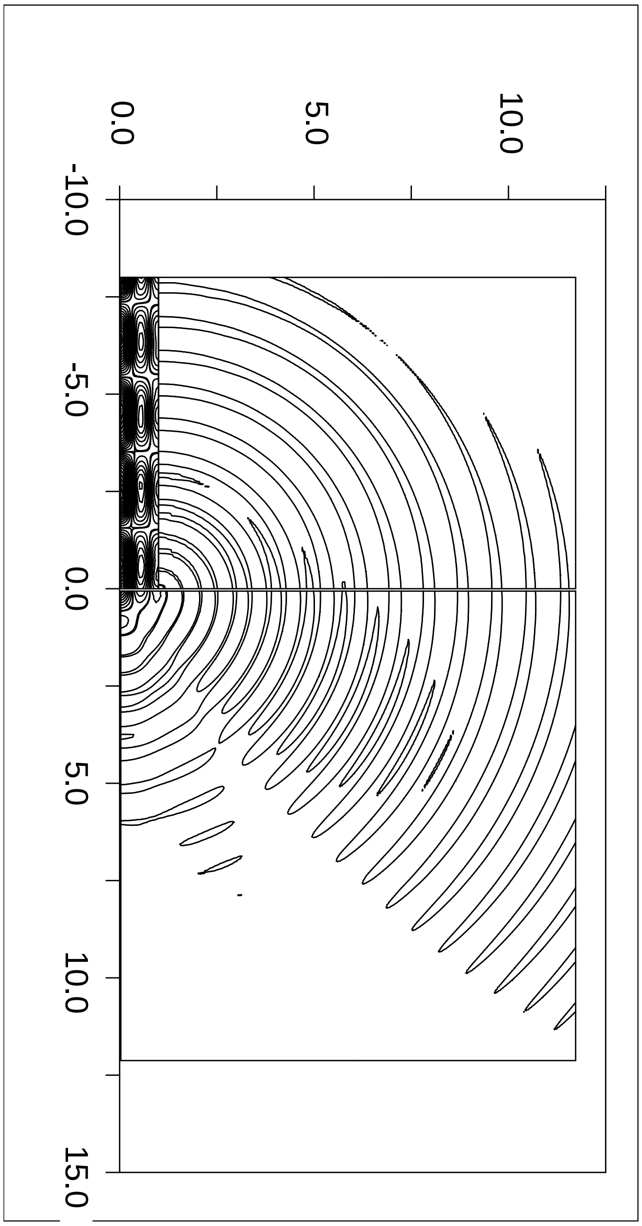

Figure 12: Instantaneous pressure contours for $\omega = 7.2$ at $t = 140$.

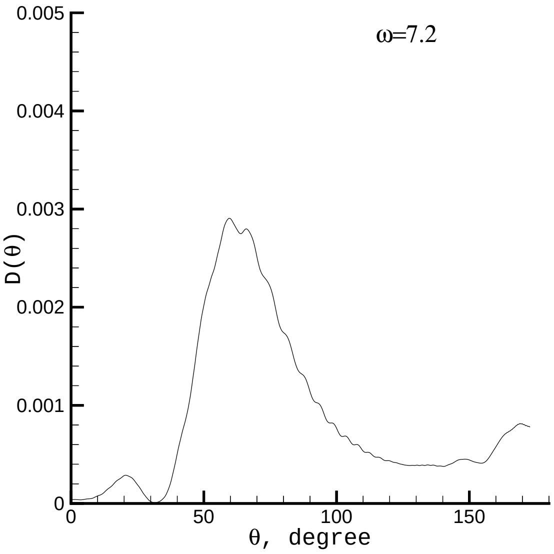

Figure 13: Far field directivity for $\omega = 7.2$.

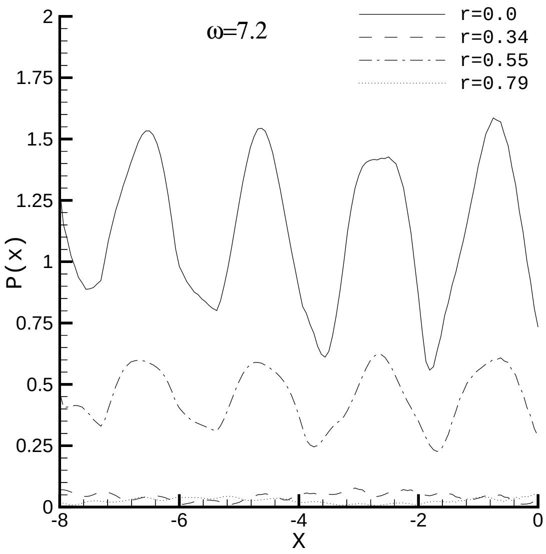

Figure 14: Wave envelope inside a duct for $\omega = 7.2$.

References

[1] Bayliss, A., and Turkel, E., "Far Field Boundary Conditions for Compressible Flows,"*J. Computational Physics*, Vol.48, Nov. 1982, pp.182-199.

[2] Dong, T. Z., Povinelli, L. A., "On Computations of Duct Acoustics with Near Cut-off Frequency," in the *Second Computational Aeroacoustics (CAA) Workshop on Benchmark Problems*, NASA CP-3352, June 1997, pp.247-257.

[3] Dong, T. Z., Shih, S. H., Mankbadi, R. R., and Povinelli, L. A., "A Numerical Study of Duct Geometry Effect on Radiation of Engine Internal Noise," AIAA-97-1604, 1997.

[4] Eversman, W., Parret, A. V., Preisser, J. S., and Silcox, R. J., "Contributions to the Finite Element Solution of the Fan Noise Radiation Problem," *Transactions fo the ASME*, Vol. 107, April 1985, pp. 215-223.

[5] Michel Guivarch, Christophe Lambert, Jean-Paul Devos, "A Computational Tools for Industrial Aeroacoustic Applications," AIAA 98-2331, June, 1998.

[6] Hardin, J.C., Ristorcelli, J.R., and Tam, C.K.W., Eds. *ICASE/LaRC Workshop on Bechmark Problems in Computaional Aeroacoutics (CAA)*, NASA CP-3300, Hampton, VA, May 1995.

[7] Hariharan, S. I. , Bayliss, Alvin, "Radiation of Sound from Unflanged Cylindrical Ducts," *SIAM J. Sci. Stat. Comput.*, Vol. 6, No. 2, April 1985, pp. 285-296.

[8] Hu, F.Q., "On Absorbing Boundary Conditions for Linearized Euler Equations by a Perfectly Matched Layer,"*J. Computational Physics*, Vol.129, 1996, pp.201-219.

[9] Hu, F. Q., Hussaini, M. Y., and Manthey, J. L., "Low-Dissipation and Low-Dispersion Runge-Kutta Schemes for Computational Acoustics," *J. Computational Physcs*, Vol.124, 1996, pp.177-191.

[10] Hu, F. Q., and Manthdy, J. L., "Application of PML Absorbing Boundary Conditions to the Benchmark Problems of Computational Aeroacoustics," in the *Second Computational Aeroacoustics (CAA) Workshop on Benchmark Problems*, NASA CP-3352, June 1997, pp.119-151.

[11] Kurbatskii, K.A., and Tam, C.K.W., "Cartesian Boundary Treatment of Curved Walls for High-Order Computational Aeroacoustics Schemes," *AIAA J.*, Vol.35, No.1, 1997, pp.133-140.

[12] Li, X.D., and Delfs, J., "Towards the Numerical Simulation of Airfoil Noise," DLR IB-129-98/1, Braunschweig, Jan. 1998.

[13] Mani, R., "Refraction of Acoustic Duct Waveguide Modes by Exhaust Jets," *Quarterly of Appl. Math.*, Vol.30, Jan. 1973, pp. 501-519

[14] Myers, M.K., "Boundary Integral Formulations for Ducted Fan Radiation Calculations," CEAS/AIAA Paper 95-076, 1995.

[15] Yusuf Özyörük and Lyle N. Long, "Multigrid Acceleration of a High-Resolution Computational Aeroacoustics Scheme," *AIAA Journal*, Vol.35, No.3, 1997, pp.428-433.

[16] Parret, A. V., and Eversman, W., "Wave Envelope and Finite Element Approximations for Turbofan Noise Radiation in Flight," *AIAA Journal*, Vol.24, No. 5, 1986, pp. 753-760.

[17] Tam, C.K.W., and Hardin, J.C., *Second Computational Aeroacoustics (CAA) Workshop on Benchmark Problems*, NASA CP-3352, June 1997.

[18] Tam, C.K.W., Kurbatskii, K.A., and Fang, J., "Numerical Boundary Conditions for Computational Aeroacoustics Benchmark Problems," in the *Second Computational Aeroacoustics (CAA) Workshop on Benchmark Problems*, NASA CP-3352, June 1997, pp.191-219.

[19] Tam, C.K.W., and Webb, J.C., "Dispersion-Relation-Preserving Finite Difference Schemes for Computational Acoustics," *J. Computational Physics*, V.107, 1993, pp.262-281.

[20] Tam, C.K.W., Webb, J.C., and Dong, T.Z., "A Study of the Short Wave Components in Computational Acoustics," *J. Computational Acoustics*, Vol.1, 1993, pp.1-30.

[21] Tam, C.K.W. and Dong, Z., "Wall Boundary Condtions for High-Order Finite Difference Schemes in Computational Aeroacoustics," *Theoretical and Computational Fluid Dynamics*, Vol.8, No.6, 1994, pp.303-322.